Optimizing for an arbitrary Schrödinger cat state. II. Application in the presence of dissipation

Matthias G. Krauss,[1,2] Daniel M. Reich,[2] and Christiane P. Koch[2,1,*]

[1] *Theoretische Physik, Universität Kassel, Heinrich-Plett-Straße 40, 34132 Kassel, Germany*
[2] *Dahlem Center for Complex Quantum Systems and Fachbereich Physik, Freie Universität Berlin, Arnimallee 14, D-14195 Berlin, Germany*

We extend here the optimization functional targeting arbitrary cat states, derived in the companion paper, to open quantum system dynamics. Applying it to a Jaynes-Cummings model with decay on the oscillator, we find, for strong dissipation and large cat radii, a change in the control strategy for preparing an entangled cat state. Our results illustrate the versatility of the quantum optimal control toolbox for practical applications in the quantum technologies.

I. INTRODUCTION

Quantum optimal control theory has established itself as a key enabling tool in the quantum technologies [1, 2]. It refers to a set of methods to devise the shapes of external electromagnetic fields that manipulate quantum dynamical processes in the best way possible [1, 2]. In the present era of noisy quantum devices, it is imperative to account for the sources of noise when deriving pulse shapes for practical applications. Decay and dephasing processes due to couplings between the quantum system and its environment constitute a major such source, and much effort has been devoted to adapting optimal control theory to open quantum systems [3]. This entails, besides the obvious replacement of Hilbert space vectors by density operators and of the time-dependent Schrödinger equation by the appropriate equation of motion for the open system, also modifications of the target functional. The latter is a suitable figure of merit that allows to quantify success of the optimization; it is a functional due to its dependence on the yet unknown pulse shape that extremizes the figure of merit.

Particular care is necessary when constructing figures of merit for open quantum system evolution. For example, functionals based on state overlap fail when the target state is mixed [4]. Another subtlety arises when optimizing for a quantum gate; then the numerical effort can be significantly reduced compared to simply lifting the problem from Hilbert space to Liouville space by exploiting the fact that the target is unitary [5]. Here, we show how to adapt the optimization functional targeting arbitrary (entangled) cat states [6] to open quantum systems.

Cat states constitute an important set of quantum states, which have various applications in quantum communication [7], computation [8–11], and sensing [12]. Quantum optimal control theory has been used to derive suitable pulses for cat state preparation [13–15], relying on state overlap with a specific cat state as final-time target. In the preceding paper [6], we have constructed an optimization functional that allows for targeting *any* state that is a cat, i.e., an equal weight superposition of coherent states, respectively an entangled cat. Just as in the case of targeting an arbitrary perfect entangler instead of a specific entangling gate [16], the cat state functional allows for more flexibility during the iterative search carried out by the optimization algorithm.

In quantum optimal control, any optimization functional must take its optimal value if and only if the desired target is reached. To this end, in the present case, the functional checks whether the state of the system at final time is an eigenstate of the annihilation operator, whether it is an equally weighted superposition, and, in case of an entangled cat, whether the two subsystems are maximally entangled. Optionally, the radius of the cat, i.e., the displacement of the corresponding coherent state, may also be prescribed. This option is particularly relevant when the system is subject to decay because the maximally achievable radius will be determined by a balance between the coherent mechanism that allows for preparing the cat, e.g. a Kerr non-linearity, and the decay [17]. Furthermore, decay is likely to also impact the creation of entanglement in the preparation of entangled cat states. To account for this impact during the optimization and search for control strategies that can avoid or mitigate this effect, it is imperative to include the effect of the environment in the model and adapt the optimization functional. We do this here for the example of a Markovian master equation.

The paper is organized as follows. We briefly introduce the model, discuss the modifications required to adapt the cat state optimization functional to open quantum system evolutions and present the optimization algorithm in Sec. II. Section III is dedicated to the optimization results obtained for the preparation of an entangled cat state in a Jaynes-Cummings model with decay of the harmonic oscillator. In particular, we compare the performance of optimized pulses obtained with and without taking the decay into account. We conclude in Sec. IV.

* christiane.koch@fu-berlin.de

II. MODEL AND DISSIPATION-ADAPTED FUNCTIONALS

Similarly to our preceding paper [6], we consider a resonant Jaynes-Cummings model with an external drive on the two-level system (TLS),

$$\hat{H}(t) = \hbar g(\hat{\sigma}_+ \otimes \hat{a} + \hat{\sigma}_- \otimes \hat{a}^\dagger) + \varepsilon^*(t)\hat{\sigma}_- \otimes \hat{\mathbb{1}} + \varepsilon(t)\hat{\sigma}_+ \otimes \hat{\mathbb{1}}\,, \tag{1}$$

where $\hat{a}$ is the lowering operator acting on the harmonic oscillator (HO), $\hat{\sigma}_\pm = \hat{\sigma}_x \pm i\hat{\sigma}_y$ are the raising and lowering operators for the TLS, and g the coupling strength between the HO and the TLS. The Hamiltonian is given in a frame that rotates with the frequency of the (resonant) HO and TLS and within the rotating wave approximation. The external control is then specified by its pulse shape $\varepsilon(t)$ together with the carrier frequency, which is assumed to be resonant with HO and TLS.

In contrast to Ref. [6], we consider an open quantum system described by a Gorini-Kossakowski-Sudarshan-Lindblad master equation [18] with T_1 relaxation of the HO,

$$\frac{\mathrm{d}}{\mathrm{d}t}\hat{\rho}(t) = -i\big[\hat{H}(t), \hat{\rho}(t)\big] + \kappa\Big(\hat{L}\hat{\rho}\hat{L}^\dagger - \frac{1}{2}\big\{\hat{L}^\dagger\hat{L}, \hat{\rho}(t)\big\}\Big)\,, \tag{2}$$

where $\hat{\rho}$ is the joint density operator of HO and TLS and $\hat{L} = \hat{\mathbb{1}} \otimes \hat{a}$ with decay rate κ.

As in Ref. [6], optimization will target an entangled cat state,

$$|\Psi_{\mathrm{cat}}\rangle = \frac{1}{\sqrt{2}}\big(\,|b_+\rangle \otimes |\psi^+_{\mathrm{cat}}\rangle + |b_-\rangle \otimes |\psi^-_{\mathrm{cat}}\rangle\,\big)\,. \tag{3}$$

When considering open system evolution, we need to adapt the optimization functional derived in Ref. [6], in particular its final time part J_T targeting arbitrary cat states,

$$J_{\mathrm{T}} = J_{\mathrm{cs}} + J_{\mathrm{cat}} + J_{|\alpha|}\,, \tag{4}$$

to density operators. The coherent state term J_{cs} forces the state to be an eigenstate of $\hat{a}^2$, whereas J_{cat} ensures the superposition property of cat states. We have also included the optional term $J_{|\alpha|}$, allowing to prescribe a desired value of the cat state radius $|\alpha|$.

The coherent state term is simply defined in terms of the variance. For open quantum systems, it becomes

$$J_{\mathrm{cs}}(\hat{\rho}) = \mathrm{Tr}\left[\left(\hat{A}^\dagger\right)^2\hat{A}^2\hat{\rho}\right] - \left|\,\mathrm{Tr}\left[\hat{A}^2\hat{\rho}\right]\right|^2, \tag{5}$$

where $\hat{A} \equiv \hat{\mathbb{1}}\otimes\hat{a}$. Using the definition of the partial trace, this is equivalent to

$$J_{\mathrm{cs}}(\hat{\rho}) = \mathrm{Tr}\left[\hat{a}^2\hat{\rho}_{\mathrm{HO}}\left(\hat{a}^\dagger\right)^2\right] - \left|\,\mathrm{Tr}\left[\hat{a}^2\hat{\rho}_{\mathrm{HO}}\right]\right|^2, \tag{6}$$

where $\hat{\rho}_{\mathrm{HO}} = \mathrm{Tr}_{\mathrm{TLS}}[\hat{\rho}]$ is the reduced state of the HO. Analogously to Ref. [6], the coherent state term can be normalized to counter the tendency towards $|\alpha| \to 0$,

$$J_{\mathrm{cs}}(\hat{\rho}) = 1 - \frac{\left|\,\mathrm{Tr}\left[\hat{a}^2\hat{\rho}_{\mathrm{HO}}\right]\right|^2}{\mathrm{Tr}\left[\hat{a}^2\hat{\rho}_{\mathrm{HO}}\left(\hat{a}^\dagger\right)^2\right]}\,. \tag{7}$$

Similarly, the term to fix the value of $|\alpha|$, $J_{|\alpha|}(\hat{\rho})$, is simply obtained from Ref. [6] by replacing the definition of expectation values,

$$J_{|\alpha|}(\hat{\rho}) = f\big(|\alpha|\big) = \frac{(|\alpha|^4 - |\alpha_{\mathrm{tgt}}|^4)^2}{|\alpha_{\mathrm{tgt}}|^8} + \frac{(|\alpha| - |\alpha_{\mathrm{tgt}}|)^2}{|\alpha_{\mathrm{tgt}}|^2}. \tag{8}$$

Finally, J_{cat} ensures equal weights in the superposition (3), which in Ref. [6] is achieved by making use of the subspace purity. This is not as straightforward to generalize to open system evolution. When optimizing coherent dynamics, the purity of either of the subsystems suffices to determine if the final state is maximally entangled. However, in the case of non-unitary evolution, the subsystem purity is not only reduced by entangling the two systems, but also decreases due to dissipation. As a result, the purity of a single subsystem is no longer an adequate measure for entanglement between the subsystems. Nevertheless, we can still use the fact that the set of target states is maximally entangled, expressing $J_{\mathrm{cat}}(\hat{\rho})$ in terms of the mutual information which, in general, is defined as

$$\mathcal{I}\big(\mathrm{HO}:\mathrm{TLS}\big) = S(\hat{\rho}_{\mathrm{HO}}) + S(\hat{\rho}_{\mathrm{TLS}}) - S(\hat{\rho}) \tag{9}$$

with $S(\hat{\rho})$ the von Neumann entropy, $S(\hat{\rho}) = -\,\mathrm{Tr}[\hat{\rho}\ln\hat{\rho}]$. For our purposes, the von Neumann entropy is inconvenient since gradient-based optimization relies on the derivative of the functional and the derivative of $S(\hat{\rho})$ is not always defined. We use the linear entropy [19, 20] instead,

$$S_{\mathrm{lin}}(\hat{\rho}) = 1 - \mathcal{P}(\hat{\rho}) = 1 - \mathrm{Tr}[\hat{\rho}^2]\,. \tag{10}$$

Accounting for the fact that all terms in the final time functional will be minimized, we obtain

$$\begin{aligned} J_{\mathrm{cat}}(\hat{\rho}) &= 1 - \Big(S_{\mathrm{lin}}(\hat{\rho}_{\mathrm{HO}}) + S_{\mathrm{lin}}(\hat{\rho}_{\mathrm{TLS}}) - S_{\mathrm{lin}}(\hat{\rho})\Big) \\ &= \mathcal{P}(\hat{\rho}_{\mathrm{HO}}) + \mathcal{P}(\hat{\rho}_{\mathrm{TLS}}) - \mathcal{P}(\hat{\rho}) \end{aligned} \tag{11}$$

in order to ensure equal-weights in the targeted superposition.

Similarly to the preceding paper [6], we use Krotov's method [21, 22] to minimize the functional. The update equation in Liouville space is given by [5, 23–25]

$$\varepsilon^{(k+1)}(t) = \varepsilon^{(k)}(t) + \frac{S(t)}{\lambda_a} \mathfrak{Re}\left\{ \left\langle \hat{\chi}^{(k)}(t),\ \frac{\partial \mathcal{L}}{\partial \varepsilon}\Big|_{\varepsilon^{(k+1)}(t)} \hat{\rho}^{(k+1)}(t) \right\rangle \right\}, \tag{12}$$

where $\frac{\partial \mathcal{L}}{\partial \varepsilon}$ is the derivative of the Liouvillian $\mathcal{L}$ with respect to the pulse ε. In case of the Hamiltonian in Eq. (1), the derivative applied to $\hat{\rho}^{(k+1)}(t)$ is given by

$$\frac{\partial \mathcal{L}}{\partial \varepsilon}\Big|_{\varepsilon^{(k)}(t)} \hat{\rho}^{(k+1)}(t) = -i\left[\hat{\sigma}_+ \otimes \mathbb{1}, \hat{\rho}^{(k+1)}(t)\right]. \tag{13}$$

The costates $\hat{\chi}^{(k)}(t)$ and $\hat{\rho}^{(k+1)}(t)$ are obtained by solving the equations of motion,

$$\frac{\mathrm{d}}{\mathrm{d}t}\hat{\rho}^{(k+1)}(t) = \mathcal{L}\left[\varepsilon^{(k+1)}(t)\right]\hat{\rho}^{(k+1)}(t) \tag{14a}$$

$$\frac{\mathrm{d}}{\mathrm{d}t}\hat{\chi}^{(k)}(t) = \mathcal{L}^{\dagger}\left[\varepsilon^{(k)}(t)\right]\hat{\chi}^{(k)}(t), \tag{14b}$$

which are propagated forward and backward in time, respectively. $\mathcal{L}\left[\varepsilon^{(k)}(t)\right]$ is the Liouvillian with the set of controls $\varepsilon^{(k)}(t)$ for the kth iteration. The boundary conditions at initial, respectively, final time for Eqs. (14) are given by

$$\hat{\rho}^{(k+1)}(0) = \hat{\rho}_0, \tag{15a}$$

$$\hat{\chi}^{(k)}(T) = -\nabla_{\hat{\rho}} J_T\Big|_{\hat{\rho}^{(k)}(T)}, \tag{15b}$$

with the initial state $\hat{\rho}_0$. Together, Eqs. (12), (14) and (15) define the iterative optimization algorithm which is started by picking a guess pulse $\varepsilon^{(0)}(t)$.

III. RESULTS

Dissipation is expected to influence the preparation process of the entangled cat states. Including this influence in the optimization framework may allow for identifying control strategies that are better adapted to the presence of dissipation than those obtained with a coherent model. In the following, we first investigate the influence of dissipation on the coherently optimized results and then reoptimize the latter to find strategies better suited for dissipative dynamics.

In order to analyze how the optimization protocols derived in Ref. [6] are affected by dissipation, we inspect three quantities, or "errors", characterizing the final state and its quality, for three different target values $|\alpha_{\mathrm{tgt}}|$ in Fig. 1. The first quantity is the deviation of the purity $\mathcal{P}$ from that of a pure state, which is equivalent to the linear entropy defined in Eq. (10). Second, in order to quantify how close the final state is to the set of target states $\left\{|\Psi_{\mathrm{cat}}\rangle\right\}$, we define a "cat infidelity",

$$I_{\mathrm{cat}}(\hat{\rho}) = \min_{|\Psi\rangle \in \{|\Psi_{\mathrm{cat}}\rangle\}} 1 - F\left(\hat{\rho}, |\Psi\rangle\langle\Psi|\right), \tag{16}$$

where

$$F(\hat{\sigma}, \hat{\rho}) = \mathrm{Tr}\sqrt{\sqrt{\hat{\rho}}\,\hat{\sigma}\,\sqrt{\hat{\rho}}} \tag{17}$$

is the state fidelity. The third quantity is the deviation of $|\alpha|$ from the target value $|\alpha_{\mathrm{tgt}}|$,

$$\Delta|\alpha| = \big||\alpha| - |\alpha_{\mathrm{tgt}}|\big|. \tag{18}$$

The target value $|\alpha_{\mathrm{tgt}}|$ determines the minimum time needed to prepare the cat state [6], the so-called quantum speed limit. We therefore discuss the influence of dissipation by expressing the dissipation strength in units of the quantum speed limit T_{QSL}. Following the same logic, the pulse duration T is chosen to be approximately twice the quantum speed limit. The specific values are $T = 2.4\pi/g$ for $|\alpha_{\mathrm{tgt}}| = 1.0$, $T = 3.5\pi/g$ for $|\alpha_{\mathrm{tgt}}| = 1.5$, and $T = 5\pi/g$ for $|\alpha_{\mathrm{tgt}}| = 2.0$.

Figure 1(a) depicts the deviation of the final state purity from the ideal purity with growing dissipation strength. The dashed lines correspond to the performance of pulses optimized for coherent evolution but evaluated in the presence of dissipation. The purity errors show a qualitatively similar behavior for different $|\alpha_{\mathrm{tgt}}|$ and, as expected, increase with dissipation strength. The solid lines display the results of reoptimization in the presence of dissipation using the pulses obtained without dissipation as guess pulse. They follow a similar trend as the coherently optimized results. Upon closer inspection, however, they exhibit improvements, which are most pronounced for $|\alpha_{\mathrm{tgt}}| = 1.5$ (magenta lines). We analyze these improvements in more detail below.

Dissipation does not only affect the purity, but we also find a larger infidelity of the final states. The cat infidelity as defined in Eq. (16) is plotted in Fig. 1(b). Analogously to Fig. 1(a), infidelity and dissipation strength are correlated and the shapes of the curves resemble those depicted in Fig. 1(a). Finally, Fig. 1(c) analyzes the error of $|\alpha|$ with respect to the target value $|\alpha_{\mathrm{tgt}}|$ as a function of the decay rate κ. Since the model accounts for decay of the harmonic oscillator, α is particularly affected by dissipation, reducing α with increasing κ. Indeed, the curves in Fig. 1(c) show this behavior and follow a similar trend as in Fig. 1(a-b) for both the coherently and the reoptimized pulses. Note that the reoptimization does not reduce the final-time cat radius error for the two larger values of $|\alpha_{\mathrm{tgt}}|$, $|\alpha_{\mathrm{tgt}}| = 1.5$ (magenta) and $|\alpha_{\mathrm{tgt}}| = 2.0$ (green). This is not surprising for the following reason. The optimization targets a sum of terms which are balanced against each other. Since the function f used in the definition of $J_{|\alpha|}$ is comparatively insensitive to errors in the desired value of $|\alpha|$, the value of $|\alpha|$ can slightly deteriorate in favor of improvements in the other terms. If needed, this could be counteracted by changing the weight of $J_{|\alpha|}$ or even changing the function f used when defining $J_{|\alpha|}$.

Despite the similar behavior of the three quantities pre-

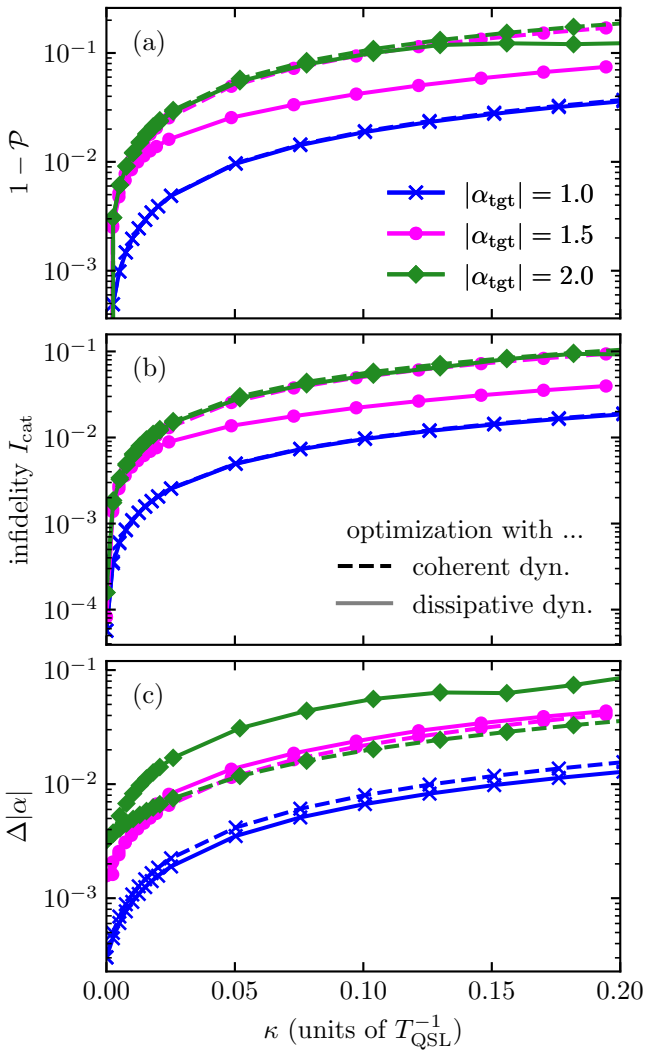

FIG. 1. Dependence of the final state errors on the dissipation strength κ for different target values $|\alpha_{\rm tgt}|$: (a) purity error, (b) cat infidelity, and (c) cat radius error. The solid lines correspond to pulses optimized with dissipation taken into account whereas the dashed lines display the results obtained using the coherently optimized pulses, but propagated with the corresponding dissipation strength.

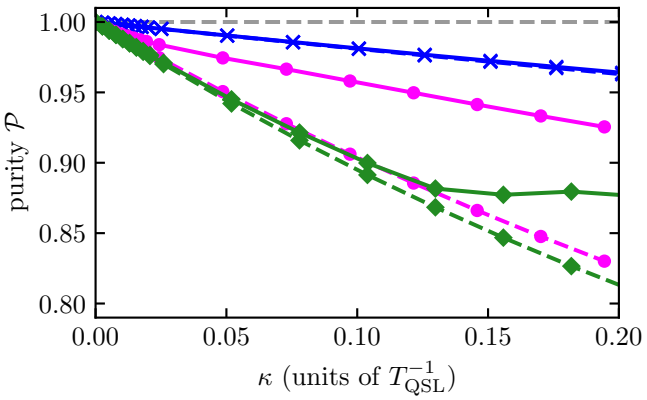

FIG. 2. The same data as in Fig. 1(a) but with linear scale for the purity to illustrate the different improvements under reoptimization with dissipation (solid) compared to coherently optimized results (dashed). Same line styles and color code as in Fig. 1.

sented in Fig. 1 on first glance, a more detailed analysis of the curves reveals three different types of adjustments that the reoptimization introduces. We illustrate these in Fig. 2 by changing the scale of plot Fig. 1(a) to highlight the differences between the coherently optimized (dashed) and reoptimized (solid) results. The blue curve, corresponding to $|\alpha_{\rm tgt}| = 1.0$, shows no improvement due to the reoptimization, which indicates that the solution found without account of dissipation is already robust. This is corroborated by the observation that the other quantities in Fig. 1(a,c) do not significantly improve either. In contrast, the purity of the reoptimized result for $|\alpha_{\rm tgt}| = 1.5$ (magenta) is strongly enhanced compared to the original result for all decay rates κ considered. An improvement under reoptimization is also observed for $|\alpha_{\rm tgt}| = 2.0$ (green), except for small values of κ. The improvement in both cases suggests that the strategies found by the coherent optimization are not optimal once dissipation is taken into account and indicates the importance of considering dissipation in the optimization for obtaining more robust strategies.

We investigate the change in control strategy next. To this end, we focus on the results for $|\alpha_{\rm tgt}| = 1.5$ and $|\alpha_{\rm tgt}| = 2.0$, showing signs of a strategy change as discussed above. To analyze the dynamics of the harmonic oscillator, the mean number of excitations,

$$\langle \hat{n} \rangle \equiv \mathrm{Tr}\left[(\hat{\mathbb{1}} \otimes \hat{n})\hat{\rho}(t)\right], \tag{19}$$

is plotted over time in Fig. 3(a-b). Analogously Fig. 3(c-d) shows the average excitation of the TLS,

$$\langle \hat{\sigma}_z \rangle \equiv \mathrm{Tr}\left[(\hat{\sigma}_z \otimes \hat{\mathbb{1}})\hat{\rho}(t)\right], \tag{20}$$

as a function of time. Additionally, the interaction between the subsystems is analyzed in Fig. 3(e-f) by means of the mutual information, defined in Eq. (9). We start by describing the dynamics for the case $|\alpha_{\rm tgt}| = 1.5$. In Fig. 3(a), the dynamics optimized under pulses with and without dissipation show clear differences. Under the coherently optimized pulses (dashed line), the HO gets excited already shortly after the beginning. In contrast, the pulse optimized taking dissipation into account (solid line) keeps the excitation in the harmonic oscillator very small until $t \approx T/2$, where it starts to increase linearly to $\langle \hat{n} \rangle \approx |\alpha|^2$. Overall, the excitation induced by the pulse optimized without dissipation is above the one for the reoptimized pulse at all times. The strategy of reducing excitation is not surprising as more excitation in the harmonic oscillator is directly related to a stronger decay. The excitation dynamics in the two level system, depicted in Fig. 3(c), is oscillatory and does not

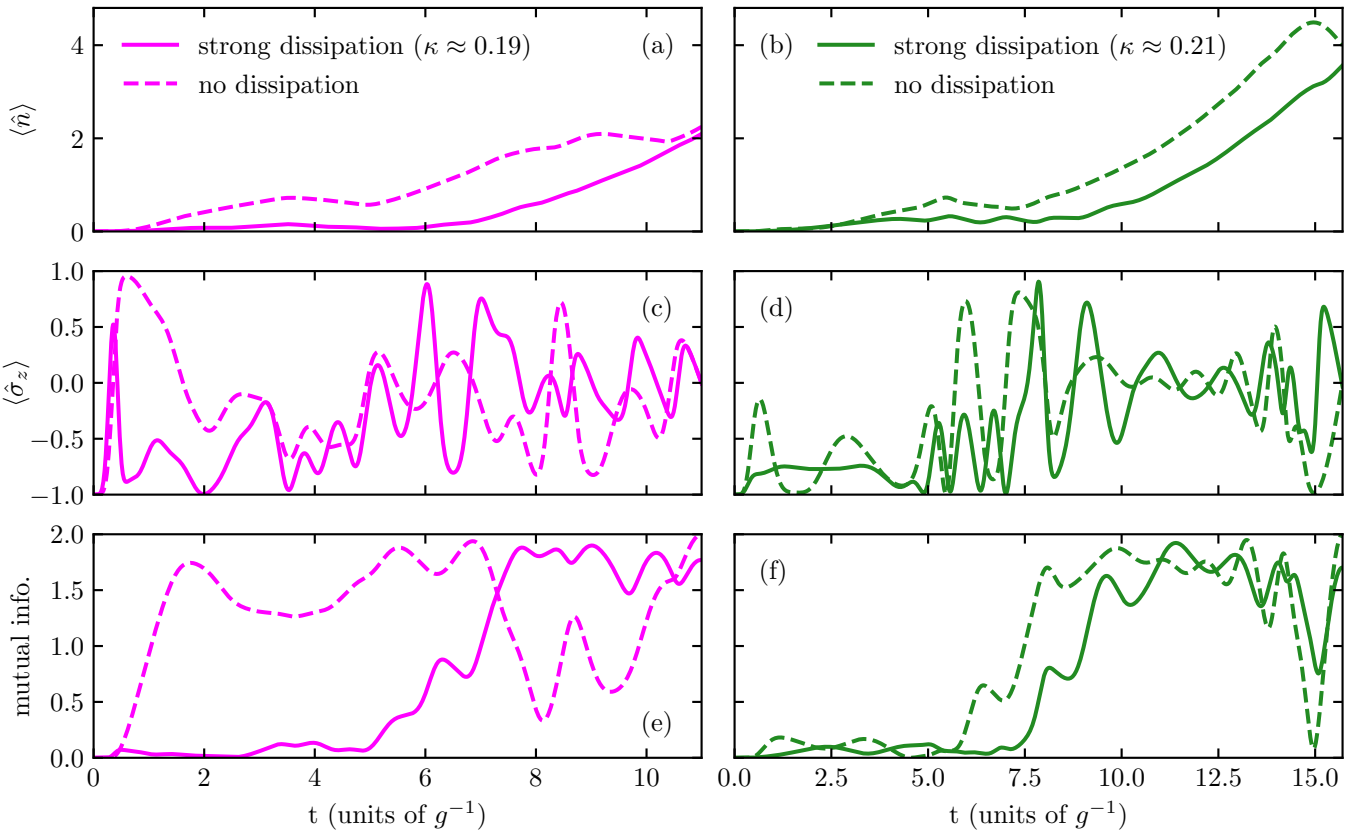

FIG. 3. Comparison of different strategies: The solid lines depict the dynamics induced by the pulse optimized with strong dissipation and the dashed lines depict the dynamics with the coherently optimized pulses. The left and right column correspond to $|\alpha_{\text{tgt}}| = 1.5$ and $|\alpha_{\text{tgt}}| = 2.0$, respectively. The panels (a-b) and (c-d) show the average excitation of the harmonic oscillator, Eq. (19), and of the two-level system, Eq. (20), respectively, as well as the mutual information in (e-f), Eq. (9).

immediately reveal an underlying strategy. As we will see below, it is important that, for strong dissipation, $\langle \hat{\sigma}_z \rangle$ oscillates around zero in the last third of the time interval. Fig. 3(e) depicts the mutual information and thus the entanglement between the subsystems. While in the coherently optimized case the harmonic oscillator and two-level system become strongly entangled from the beginning, the strategy for the reoptimized pulses is to keep the subsystems disentangled until about $t \approx T/2$, and then continue to almost full entanglement. This is also corroborated by the value of $\langle \hat{\sigma}_z \rangle \approx 0$ in Fig. 3(c), indicating that the system is close to a maximally entangled state, which allows excitation transfer directly to the harmonic oscillator, and also explains the straight excitation increase in Fig. 3(a). All in all, the strategy identified by the optimization algorithm in the presence of dissipation is to wait in the beginning and then generate the cat state as fast as possible in the end. This simply reduces the time during which excitation in the harmonic oscillator is exposed to decay, yielding higher quality final states.

In case of $|\alpha_{\text{tgt}}| = 2.0$, the strategy change is more subtle. For both curves in Fig. 3(b), $\langle \hat{n} \rangle$ is almost constant around zero in the beginning and linearly grows to the desired value of $\langle \hat{n} \rangle_{\text{tgt}} = |\alpha_{\text{tgt}}|^2 = 4.0$ after about half of the time. The difference between both curves is the final peak of the dynamics under the coherently optimized pulse (dashed line), which surpasses the desired value just before the end and finally decreases to match the desired excitation. In contrast, the solid curve, representing the dynamics under the reoptimized pulse, approaches the final value in an almost straight line, a behavior already observed for the reoptimized dynamics in Fig. 3(a). The dynamics of $\langle \hat{\sigma}_z \rangle$, depicted in Fig. 3(d), is again more complex. The first part is clearly dominated by small fluctuations around the ground state of the two-level system. Around half time, both dynamics exhibit strong oscillations before $\langle \hat{\sigma}_z \rangle$ remains close to zero in the interval between $t \approx 10\, g^{-1}$ and $t \approx 13\, g^{-1}$. Thereafter, the oscillations grow stronger again, ultimately ending close to the desired value of $\langle \hat{\sigma}_z \rangle = 0$. Finally, the dynamics of the mutual information in Fig. 3(f) are similar to each other and those found for the dissipatively optimized dynamics in Fig. 3(e). For the pulse obtained under strong dissipation, the mutual information increases a bit later compared to the coherently optimized case. Also, the mutual information for $|\alpha_{\text{tgt}}| = 2.0$ exhibits a significant dip just before the end, which indicates that the system

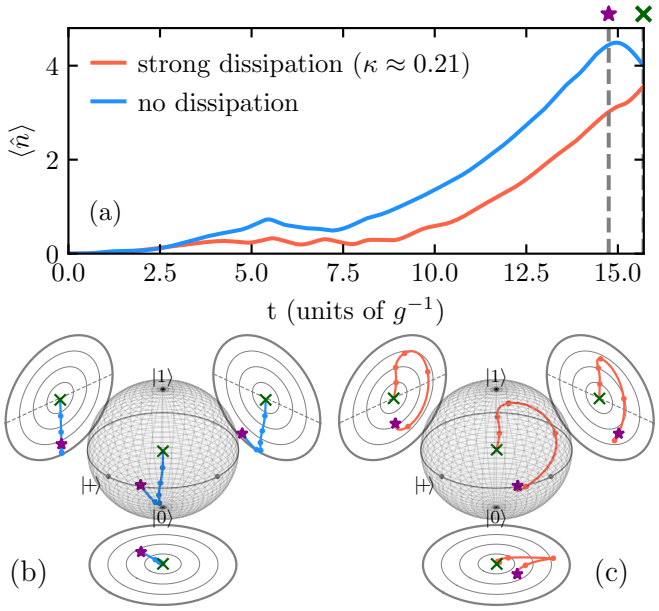

FIG. 4. Visualization of the strategy change, storing excitation in the two-level system instead of the harmonic oscillator, when optimizing with strong dissipation. Panel (a) is the same plot as in Fig. 3(b) and panels (b-c) show the dynamics of the TLS in Bloch sphere representation. For the sake of clarity, we only show the final part of the dynamics in (b-c), as indicated by the gray dashed lines in (a).

goes to a pure state just before the entangled cat state is created. Apart from this detail, both strategies for $|\alpha_{\text{tgt}}| = 2.0$ follow a similar structure as the reoptimized dynamics discussed in Fig. 3(e). Despite this similarity of the dynamics, we observe a strong improvement in purity and even fidelity for large dissipation. The mutual information of the reoptimized pulse in Fig. 3(e) also exhibits a speedup, compared to the coherently optimized dynamics, which is reflected in the delayed rise of the solid curve, compared to the dashed one. However, since the speedup is only marginal, the enhancement must also be related to avoiding the final peak in the average excitation of the harmonic oscillator.

To further illustrate the strategy change for $|\alpha_{\text{tgt}}| = 2.0$, the TLS dynamics close to the final peak is presented in Fig. 4(b-c) together with the data from Fig. 3(b) replotted in Fig. 4(a) for clarity. Here, the star and cross in Fig. 4(a) indicate the time period plotted in Fig. 4(b-c). For the optimization not taking into account dissipation (Fig. 4(b)), the TLS starts by evolving to the ground state $|0\rangle$ becoming disentangled from the harmonic oscillator as already indicated by the dip in the mutual information in Fig. 3(e). It continues and evolves to the maximally entangled state at the center of the Bloch sphere. For the reoptimized dynamics (Fig. 4(c)), the TLS instead starts to evolve towards the excited state $|1\rangle$, but does not completely reach it, due to the purity reduction caused by dissipation. From there it evolves to the center of the Bloch sphere, again in an almost straight line. We thus find that the two strategies approach the maximally entangled final state in a similar way, yet from different sides of the Bloch sphere. In the case of the coherently optimized pulse (blue), this means that for the final part of the protocol, excitation is transferred from the harmonic oscillator to the two-level system. This coincides with the observation of the peak around $t = 15\, g^{-1}$ in Fig. 4(a). It represents the excitation excess that is stored in the HO and later transferred to the two-level system. Since the dissipation punishes more excitation in the harmonic oscillator, the strategy for the reoptimized pulse is to instead store excitation in the two-level system and transfer the surplus excitation to the harmonic oscillator in the end, thus protecting it from decay as long as possible.

IV. CONCLUSIONS

We have generalized the optimization framework for targeting arbitrary entangled cat states [6] to open quantum system dynamics. The main modification required to this end was to replace the subsystem purity as a measure for entanglement between the subsystems by the (linear) entropy. We have then investigated the influence of dissipation on the creation of arbitrary entangled cat states in a Jaynes-Cummings model, comparing the performance of coherently optimized pulses [6] with those optimized in the presence of decay of the harmonic oscillator. Accounting for the decay during the optimization has allowed us to improve the final state fidelity for states with large cat radius which are most affected by the decay.

Inspecting the dynamics under the optimized pulses, we have been able to identify the strategy changes obtained when taking dissipation into account. In the presence of decay, it is more advantageous to keep excitation of the harmonic oscillator low as long as possible. While this by itself is not surprising, the optimization identifies the most suitable protocol depending on the desired cat radius. For sufficiently small radii, the cat is simply generated as fast as possible towards the end of the protocol. For larger cat radii, the best way to keep the oscillator excitation low is by storing excitation temporarily in the two-level system. These results illustrate how taking dissipation into account during the optimization of a desired quantum process allows for identifying control strategies which are more robust than those obtained by optimizing coherent dynamics.

In future work, it will be interesting to apply the cat state optimization framework derived here to open quantum systems that require a description of the environment's influence beyond a phenomenological decay, in particular to systems with non-Markovian dynamics. For example, superconducting circuits are subject to $1/f$ noise [26] which results in non-Markovian dynamics. Beyond identifying strategies that are best adapted to the open system properties, this may allow for exploiting

non-Markovianity as a resource for control, see e.g. [3, 27] and references therein. The present results thus increase the utility of the quantum optimal control toolbox [1, 2] for practical applications in the quantum technologies.

ACKNOWLEDGMENTS

Financial support from the federal state of Hesse, Germany via the SMolBits project within the LOEWE program is gratefully acknowledged.

[1] S. J. Glaser, U. Boscain, T. Calarco, C. P. Koch, W. Köckenberger, R. Kosloff, I. Kuprov, B. Luy, S. Schirmer, T. Schulte-Herbrüggen, D. Sugny, and F. K. Wilhelm, Training Schrödinger's cat: Quantum optimal control: Strategic report on current status, visions and goals for research in Europe, Eur. Phys. J. D **69**, 279 (2015).

[2] C. P. Koch, U. Boscain, T. Calarco, G. Dirr, S. Filipp, S. J. Glaser, R. Kosloff, S. Montangero, T. Schulte-Herbrüggen, D. Sugny, and F. K. Wilhelm, Quantum optimal control in quantum technologies. Strategic report on current status, visions and goals for research in Europe, EPJ Quantum Technol. **9**, 19 (2022).

[3] C. P. Koch, Controlling open quantum systems: Tools, achievements, and limitations, J. Phys.: Condens. Matter **28**, 213001 (2016).

[4] D. Basilewitsch, C. P. Koch, and D. M. Reich, Quantum Optimal Control for Mixed State Squeezing in Cavity Optomechanics, Adv. Quantum Technol. **2**, 1800110 (2019).

[5] M. H. Goerz, D. M. Reich, and C. P. Koch, Optimal control theory for a unitary operation under dissipative evolution, New J. Phys. **16**, 055012 (2014).

[6] M. G. Krauss, C. P. Koch, and D. M. Reich, Optimizing for an arbitrary schrödinger cat state. I. Functionals and application to coherent dynamics, TBD (2022).

[7] S. van Enk and O. Hirota, Entangled coherent states: Teleportation and decoherence, Phys. Rev. A **64**, 022313 (2001).

[8] P. T. Cochrane, G. J. Milburn, and W. J. Munro, Macroscopically distinct quantum-superposition states as a bosonic code for amplitude damping, Phys. Rev. A **59**, 2631 (1999).

[9] M. Mirrahimi, Cat-qubits for quantum computation, Comptes Rendus Physique **17**, 778 (2016).

[10] A. Grimm, N. E. Frattini, S. Puri, S. O. Mundhada, S. Touzard, M. Mirrahimi, S. M. Girvin, S. Shankar, and M. H. Devoret, Stabilization and operation of a Kerr-cat qubit, Nature **584**, 205 (2020).

[11] Q.-P. Su, Y. Zhang, and C.-P. Yang, Single-step implementation of a hybrid controlled-not gate with one superconducting qubit simultaneously controlling multiple target cat-state qubits, Phys. Rev. A **105**, 062436 (2022).

[12] W. J. Munro, K. Nemoto, G. J. Milburn, and S. L. Braunstein, Weak-force detection with superposed coherent states, Phys. Rev. A **66**, 023819 (2002).

[13] K. Rojan, D. M. Reich, I. Dotsenko, J.-M. Raimond, C. P. Koch, and G. Morigi, Arbitrary-quantum-state preparation of a harmonic oscillator via optimal control, Phys. Rev. A **90**, 023824 (2014).

[14] N. Ofek, A. Petrenko, R. Heeres, P. Reinhold, Z. Leghtas, B. Vlastakis, Y. Liu, L. Frunzio, S. M. Girvin, L. Jiang, M. Mirrahimi, M. H. Devoret, and R. J. Schoelkopf, Extending the lifetime of a quantum bit with error correction in superconducting circuits, Nature **536**, 441 (2016).

[15] J.-J. Xue, K.-H. Yu, W.-X. Liu, X. Wang, and H.-R. Li, Fast generation of cat states in Kerr nonlinear resonators via optimal adiabatic control, New J. Phys. **24**, 053015 (2022).

[16] P. Watts, J. Vala, M. M. Müller, T. Calarco, K. B. Whaley, D. M. Reich, M. H. Goerz, and C. P. Koch, Optimizing for an arbitrary perfect entangler. I. Functionals, Phys. Rev. A **91**, 062306 (2015).

[17] B. He, M. Nadeem, and J. A. Bergou, Scheme for generating coherent-state superpositions with realistic cross-Kerr nonlinearity, Phys. Rev. A **79**, 035802 (2009).

[18] H.-P. Breuer and F. Petruccione, *The Theory of Open Quantum Systems* (Oxford University Press, Oxford ; New York, 2002).

[19] W. H. Zurek, S. Habib, and J. P. Paz, Coherent states via decoherence, Phys. Rev. Lett. **70**, 1187 (1993).

[20] G. Manfredi and M. R. Feix, Entropy and Wigner functions, Phys. Rev. E **62**, 4665 (2000).

[21] A. I. Konnov and V. F. Krotov, On global methods of successive improvement of controll processes, Autom. Remote Control **60**, 1427 (1999).

[22] V. Krotov, *Global Methods in Optimal Control Theory* (CRC Press, 1995).

[23] D. M. Reich, M. Ndong, and C. P. Koch, Monotonically convergent optimization in quantum control using Krotov's method, J. Chem. Phys. **136**, 104103 (2012).

[24] D. Basilewitsch, H. Yuan, and C. P. Koch, Optimally controlled quantum discrimination and estimation, Phys. Rev. Research **2**, 033396 (2020).

[25] M. H. Goerz, D. M. Reich, and C. P. Koch, Corrigendum: Optimal control theory for a unitary operation under dissipative evolution (2014 New J. Phys. 16 055012), New J. Phys. **23**, 039501 (2021).

[26] E. Paladino, Y. M. Galperin, G. Falci, and B. L. Altshuler, 1 / f noise: Implications for solid-state quantum information, Rev. Mod. Phys. **86**, 361 (2014).

[27] D. M. Reich, N. Katz, and C. P. Koch, Exploiting Non-Markovianity for Quantum Control, Sci Rep **5**, 12430 (2015).